Frequency Domain Lifetime Characterization

Dieter K. Schroder, *Fellow, IEEE*, Jae-Eun Park, *Member, IEEE*, Suat-Eng Tan, Byoung D. Choi, Seigo Kishino, and Haruhiko Yoshida

***Abstract*—Time-based measurements are commonly used for lifetime characterization of semiconductors. We have developed the theory, verified by experiment, of frequency-based lifetime characterization as an alternative to time-based measurements for MOS devices biased in inversion. One consideration during lifetime/diffusion length measurements, is whether the near-surface space-charge region or the bulk or quasineutral region is characterized. To characterize the near-surface space-charge region of the device, one usually makes room temperature pulsed MOS capacitor or diode leakage current measurements. We show that room-temperature, frequency-domain capacitance, conductance, or resistance measurements characterize the quasineutral bulk, not the space-charge region, in contrast to room-temperature pulsed MOS-C or diode leakage current measurements which characterize the space-charge region.**

***Index Terms*—Capacitance, impurities, MOS capacitors, semiconductor device measurements, semiconductor materials, semiconductors.**

I. Introduction

MOST semiconductor carrier lifetime or minority carrier diffusion length measurements are made in the time domain or in steady state. For example, photoconductance decay and pulsed MOS capacitor measurements are transients measurements [1], while surface photovoltage [2] and diode leakage current measurements[3] are steady state measurements. The theory and interpretation of such measurements is well in hand [4]. Frequency-dependent optically-induced lifetime measurements have been treated by Nakhmanson [5]. Some recently developed instruments for lifetime or diffusion length characterization, are based on frequency-dependent measurements of the device/material voltage or capacitance. It is, of course, well known that frequency-domain measurements contain similar information as time-domain measurements. We present here the theory and experiments for frequency-domain measurements to extract carrier lifetimes and diffusion lengths from MOS capacitors biased into inversion. We have used uncontaminated wafers, as well as samples deliberately contaminated with Fe and Au to test the theory and have, furthermore, used extensive MEDICI modeling to corroborate our analytical theory.

Manuscript received October 19, 1999; revised March 29, 2000. This work was supported in part by the Silicon Wafer Engineering and Defect Science Consortium (SiWEDS) (Komatsu Electronic Metals, MEMC Electronic Materials, Mitsubishi Silicon, SEH America, Nippon Steel, Sumitomo Sitix Silicon, and Wacker Siltronic Corporation) and by a grant from the Ministry of Education, Science, Sports, and Culture of Japan under the Grant-in-Aid for Scientific Research 10044171. The review of this paper was arranged by Editor J. N. Hollenhorst.

D. K. Schroder, J.-E. Park, S.-E. Tan, and B. D. Choi are with the Department of Electrical Engineering and Center for Solid State Electronics Research, Arizona State University, Tempe, AZ 85287-5706 USA (e-mail: schroder@asu.edu).

S. Kishino and H. Yoshida are with the Electronics Department, Himeji Institute of Technology, Himeji 671-22, Japan.

Publisher Item Identifier S 0018-9383(00)06044-5.

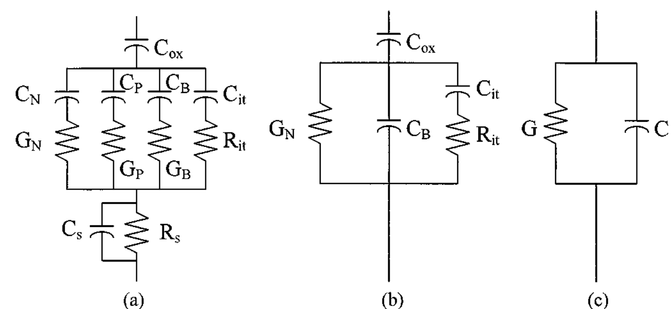

Fig. 1. (a) Equivalent circuit, (b) reduced equivalent circuit, and (c) measured circuit.

II. Theory—Analytical

The equivalent circuit concept to describe and analyze semiconductor devices has proven to be very powerful. Some of the earliest papers dealing with the equivalent circuit of the MOS capacitor are due Lehovec and Slobodskoy [6] and Hofstein and Warfield [7]. Sah gives detailed equivalent circuits of semiconductor devices [8]. A detailed discussion of equivalent circuits for MOS capacitors can be found in Nicollian and Brews [9]. We present the theory of frequency-domain measurements, by considering MOS capacitors (MOS-C). Such devices are appropriate because recent implementations of measurement techniques use Kelvin probes and/or corona charge as the "gate" electrode. Such implementations can be viewed as a form of MOS capacitor. An MOS-C is best suited for lifetime characterization when biased in inversion, because then we are concerned with minority carriers in the inversion layer and their generation and recombination. That is not the case in depletion or accumulation, where only majority carriers are important.

The MOS-C on a p-type substrate can be represented by the equivalent circuit in Fig. 1(a), consisting of the gate oxide capacitance (C_{ox}), the inversion charge capacitance (C_N), the accumulation charge capacitance (C_P), the interface trapped charge capacitance (C_{it}), and the space-charge region capacitance (C_B) as well as their corresponding conductances and the series resistance R_s and the capacitance of the substrate C_s. The R_sC_s time constant, which is the dielectric relaxation time, is important only when the lifetime is on the order of the relaxation time. This is only relevant for high resistivity material as used for Si radiation detectors, for example.

Although the device can be biased in accumulation, depletion, or inversion, we will concentrate on the inversion state in this paper. In inversion, the hole density near the surface for a p-type

0018–9383/00$10.00 © 2000 IEEE

substrate is very low, making the majority carrier capacitance C_P small allowing it to be treated as an open circuit. By the same token, the surface electron density is very high, making the inversion charge capacitance C_N high, allowing it to be replaced by a short circuit. The bulk conductance G_B of the space-charge capacitance is high due to the fast majority carrier response and we will replace it by a short circuit. Further, we will neglect the series resistance R_s. This allows the equivalent circuit to be simplified to that in Fig. 1(b).

Simplifying the circuit further to one actually determined by measurement gives Fig. 1(c) with an admittance of

$$Y = G + jB = G + j\omega C \tag{1}$$

where G is the conductance and B the susceptance. Through a straightforward but tedious circuit conversion, we find for the equivalent capacitance and conductance (2) and (3), shown at the bottom of the page, where

$$\omega_1 = \frac{G_N}{C_{ox}}; \quad \omega_2 = \frac{G_N}{C_B}; \quad \omega_3 = \frac{G_N}{C_{it}}; \quad \tau_{it} = R_{it}C_{it}. \tag{4}$$

In general, we need to consider all terms. However, for low interface trapped charge density, D_{it} and C_{it} are small ($C_{it} = qD_{it}$) allowing it to be neglected and ω_3 becomes very high, leading to

$$C = \frac{1 + \left(\frac{\omega}{\omega_2}\right)\left(\frac{\omega}{\omega_1} + \frac{\omega}{\omega_2}\right)}{1 + \left(\frac{\omega}{\omega_1} + \frac{\omega}{\omega_2}\right)^2} C_{ox};$$

$$G = \frac{\left(\frac{\omega}{\omega_1}\right)}{1 + \left(\frac{\omega}{\omega_1} + \frac{\omega}{\omega_2}\right)^2} \omega C_{ox}. \tag{5}$$

These expressions are identical to those of Baccarani *et al.* [10] if in their expression we let the inversion capacitance become very high. They show that this equivalent circuit expression gives results identical to those obtained by considering the device as a transmission line.

The low and high-frequency limits of these expressions are

$\omega \to 0$:

$$C = C_{ox}; \qquad G = \omega C_{ox} \tag{6a}$$

$\omega \to \infty$:

$$C = \frac{C_{ox}}{1 + C_{ox}/C_B}; \qquad G = \frac{G_N}{(1 + C_B/C_{ox})^2} \tag{6b}$$

leading to the C/G ratios as

$$\frac{C}{G}(\omega \to 0) = \frac{1}{\omega}; \qquad \frac{C}{G}(\omega \to \infty) = \frac{C_B(1 + C_B/C_{ox})}{G_N}. \tag{7}$$

III. Space-Charge Region and Quasineutral Region Generation

It is obvious what the capacitances in Fig. 1 are, but what are the loss elements, i.e., G_N and R_{it}? The conductance G_N represents the "generation conductance" that supplies electrons to the inversion layer with two components: space-charge region (scr) and quasineutral region (qnr) generation. R_{it} represents the loss due to recombination/generation through interface states and $R_{it}C_{it}$ represents the interface trap density time constant. We assume uniformly-doped wafers with constant diffusion length throughout the paper. For the case of nonuniform diffusion lengths (epitaxial layer or denuded zone) the analysis must be appropriately modified.

The scr generation rate G_{scr} and conductance $G_{N,\,\text{scr}}$ are

$$G_{\text{scr}} = I_{\text{scr}} = \frac{qAn_iW}{\tau_g};$$

$$G_{N,\,\text{scr}} = \frac{I_{\text{scr}}}{V} = \frac{qAn_iW}{\tau_g\phi_s} \tag{8}$$

where

- W scr width;
- τ_g generation lifetime;
- A area;
- ϕ_s the surface potential, i.e., the voltage across the semiconductor substrate.

We take the surface potential in inversion as $\phi_s = 2\phi_F = 2(kT/q)\ln(N_A/n_i)$, i.e., twice the Fermi potential. ϕ_s is actually a few kT/q higher than $2\phi_F$, but this is a minor effect which we neglect. T is the temperature, N_A is the wafer doping density and n_i the intrinsic carrier density. With W given by

$$W = \sqrt{\frac{2K_s\varepsilon_o\phi_s}{qN_A}} \tag{9}$$

we find $G_{N,\,\text{scr}}$ to be

$$G_{N,\,\text{scr}} = \frac{2K_s\varepsilon_oAn_i}{\tau_gN_AW} \tag{10}$$

which depends on the intrinsic carrier density, n_i, the doping density N_A, and the generation lifetime, τ_g.

$$C = \frac{1 + \left(\frac{\omega}{\omega_2} + \frac{\omega}{\omega_3}\right)^2 + (\omega\tau_{it})^2\left(\frac{\omega}{\omega_2}\right)\left(\frac{\omega}{\omega_1} + \frac{\omega}{\omega_2}\right) + \frac{\omega^2}{\omega_1\omega_2} + \frac{\omega^2}{\omega_1\omega_3} + 2\omega\tau_{it}\frac{\omega}{\omega_3} + (\omega\tau_{it})^2}{1 + (1 + (\omega\tau_{it})^2)\left(\frac{\omega}{\omega_1} + \frac{\omega}{\omega_2}\right)^2 + \frac{2\omega^2}{\omega_2\omega_3} + \frac{2\omega^2}{\omega_1\omega_3} + \left(\frac{\omega}{\omega_3}\right)^2 + 2\omega\tau_{it}\frac{\omega}{\omega_3} + (\omega\tau_{it})^2} C_{ox} \tag{2}$$

$$G = \frac{1 + \left(\frac{\omega}{\omega_1}\right)\left(1 + \frac{\omega}{\omega_3}\omega\tau_{it} + (\omega\tau_{it})^2\right)}{1 + (1 + (\omega\tau_{it})^2)\left(\frac{\omega}{\omega_1} + \frac{\omega}{\omega_2}\right)^2 + \frac{2\omega^2}{\omega_2\omega_3} + \frac{2\omega^2}{\omega_1\omega_3} + \left(\frac{\omega}{\omega_3}\right)^2 + 2\omega\tau_{it}\frac{\omega}{\omega_3} + (\omega\tau_{it})^2} \omega C_{ox} \tag{3}$$

The quasineutral region generation rate $G_{\rm qnr}$ and conductance $G_{N,\,\rm qnr}$ are [9]

$$G_{\rm qnr} = I_{\rm qnr} = \frac{qAn_i^2 D_n}{N_A L_n};$$
$$G_{N,\,\rm qnr} = \frac{I_{\rm qnr}}{V} = \frac{qAn_i^2 D_n/N_A L_n}{kT/q} = \frac{qA\mu_n n_i^2}{N_A L_n} \quad (11)$$

where D_n is the electron diffusion constant and μ_n the electron mobility. We have used the voltage drop across the qnr region as kT/q, appropriate for the voltage drop due to minority carrier diffusion and L_n is the minority carrier diffusion length $(L_n = (D_n \tau_r)^{1/2})$ with τ_r the recombination lifetime. For the diffusion length, we simply use L_n. This implies that the wafer is at least three to four diffusion lengths thick. If that is not the case, then we need to use a modified diffusion length [11]. Our approximation, however, does not affect the theory developed here.

The recombination and generation lifetimes are taken to be $\tau_r = \tau_{ro}/(1+j\omega\tau_{ro})$ and $\tau_g = \tau_{go}/(1+j\omega\tau_{go})$ in our analysis. This modification from the standard lifetimes of τ_r and τ_g is due to the ac signal excitation and can be derived from the ac continuity equation [12]. For simplicity, we have taken τ_{go} as constant with temperature, although it is approximately given by $\tau_{go} \approx \tau_{ro} \exp[(E_T - E_i)/kT]$ [13]. Our results indicate that neither the capacitance nor the conductance is sensitive to the generation lifetime for the conditions we use. τ_{go} decreases with temperature, according to the equation above, but since we do not know $E_T - E_i$ in general, we have neglected this dependence here.

The total generation/recombination conductance is

$$G_N = G_{N,\,\rm scr} + G_{N,\,\rm qnr} = \frac{2K_s\varepsilon_o A n_i}{\tau_g N_A W} + \frac{qA\mu_n n_i^2}{N_A L_n} \quad (12)$$

Using

$$C_{ox} = \frac{K_{ox}\varepsilon_o A}{t_{ox}}; \quad C_B = \frac{K_s\varepsilon_o A}{W}; \quad C_{it} = qAD_{it}. \quad (13)$$

in combination with (12), allows the various frequencies to be expressed as

$$\omega_1 = \frac{2K_s n_i t_{ox}}{K_{ox}\tau_g N_A W} + \frac{q\mu_n n_i^2 t_{ox}}{K_{ox}\varepsilon_o N_A L_n};$$
$$\omega_2 = \frac{2n_i}{\tau_g N_A} + \frac{q\mu_n n_i^2 W}{K_s\varepsilon_o N_A L_n};$$
$$\omega_3 = \frac{2K_s\varepsilon_o n_i}{q\tau_g N_A W D_{it}} + \frac{\mu_n n_i^2}{N_A L_n D_{it}}. \quad (14)$$

Here, t_{ox} is the oxide thickness.

To see the behavior of scr and qnr generation, we plot in Fig. 2 the capacitance and conductance calculated with (5). The conductance is shown as G in Fig. 2(a) and as G/ω in Fig. 2(b). To determine the lifetime, we need to know the break frequencies ω_1 or ω_2. ω_1 cannot be readily determined from either capacitance or conductance. However, ω_2 can be obtained from the capacitance as the lower breakpoint. The mid frequency $\omega_{\rm mid} = \omega_1\omega_2/(\omega_1+\omega_2)$, readily determined as the midpoint on the capacitance and the breakpoint on the conductance curves as well as the breakpoint on the G/ω curve, is

$$\omega_{\rm mid} = \frac{G_N}{C_{ox}+C_B} = \frac{2n_i/\tau_g + q\mu_n n_i^2 W/K_s\varepsilon_o L_n}{N_A(1+K_{ox}W/K_s t_{ox})}. \quad (15)$$

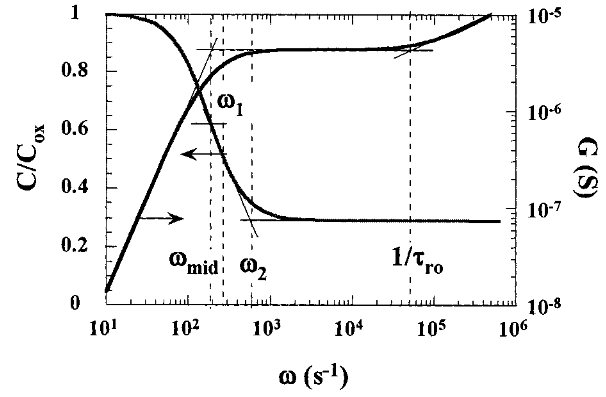

(a)

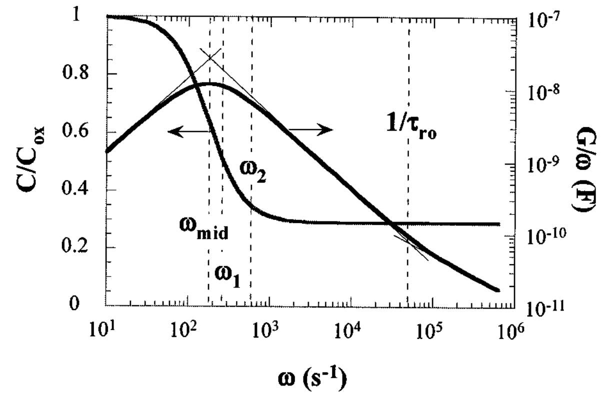

(b)

Fig. 2. Capacitance, conductance, and conductance/ω as a function of radian frequency. $\tau_{ro} = 20$ μs, $\tau_{go} = 1$ ms, $N_A = 10^{15}$ cm^{-3}, $t_{ox} = 100$ nm, $T = 370$ K, $A = 1$ cm^2.

The inverse lifetime τ_{ro} is easiest determined from the second breakpoint on the $G-\omega$ and the $G/\omega - \omega$ curves. It is obvious from (15) that neither τ_g nor L_n is easily extracted from $\omega_{\rm mid}$, unless one knows which of the two terms in the numerator dominates.

In order to extract lifetime/diffusion length, we need to know how C and G depend on various material/device parameters. One parameter frequently varied is temperature to change the generation rate. Here, we must be very careful to point out what is measured. During diode leakage current and pulsed MOS capacitor lifetime measurements, one measures in effect the *generation rate*, G, because both capacitance transient decay and diode leakage current depend directly on the generation rate.

In Fig. 3, we show the dependence of generation rates $G_{\rm scr}$ and $G_{\rm qnr}$ on temperature, using $\tau_{ro} = 20$ μs, corresponding to a low-frequency room-temperature diffusion length of approximately 250 μm, $\tau_{go} = 1$ ms, and the generally accepted temperature dependence for n_i and μ_n [1]. As is well known from measurements such as junction leakage current or pulsed MOS capacitor recovery time, carrier generation is determined by scr generation at temperatures around room temperature and by qnr generation at higher temperatures. The former is proportional to n_i and the latter to n_i^2, making the temperature behavior distinctly different in the various temperature ranges. The breakpoint temperature in this example in Fig. 3 is $T = 325$ K. Above

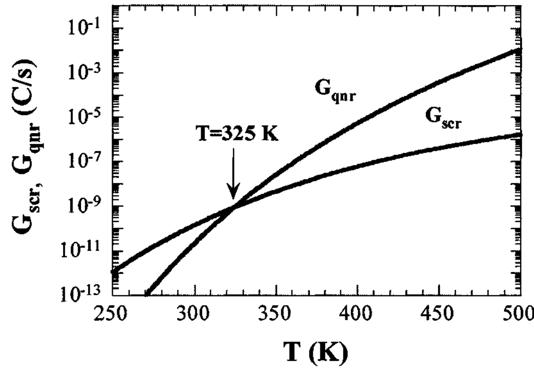

Fig. 3. Space-charge region and quasineutral region generation rates versus temperature. $\tau_{ro} = 20$ μs, $\tau_{go} = 1$ ms, $N_A = 10^{15}$ cm^{-3}.

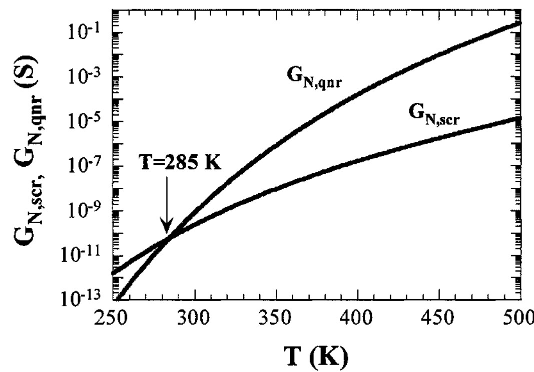

Fig. 4. Space-charge region and quasineutral region conductances versus temperature. $\tau_{ro} = 20$ μs, $\tau_{go} = 1$ ms, $N_A = 10^{15}$ cm^{-3}.

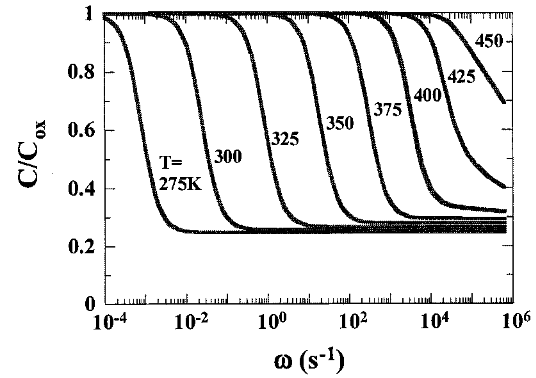

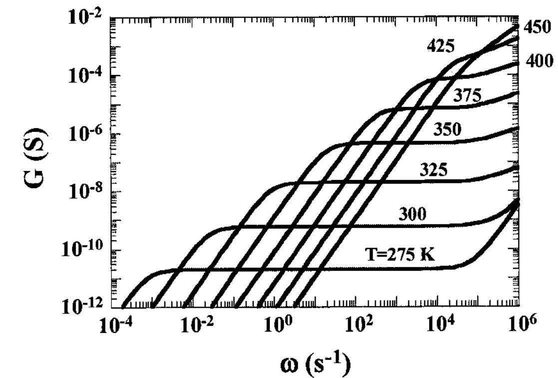

Fig. 5. Capacitance and conductance versus radian frequency as a function of temperature. $\tau_{ro} = 20$ μs, $\tau_{go} = 1$ ms, $N_A = 10^{15}$ cm^{-3}, $t_{ox} = 100$ nm, $A = 1$ cm^2.

325 K, generation is dominated by quasineutral region generation, determined by the diffusion length, but, around room temperature, scr generation dominates, governed by the generation lifetime.

How do scr and qnr *conductances* behave as a function of temperature? One might expect them to exhibit the same temperature behavior as the generation rates. Surprisingly, this is not true, as illustrated in Fig. 4. The breakpoint between scr and qnr domination occurs at T =285 K, significantly lower than the generation rate breakpoint of T =325 K. Hence, those measurements that rely on conductance or capacitance measurements as a function of frequency and confine their measurements to room temperature or above, find the device behavior *dominated by qnr generation*.

One might ask, so what? Well, if, for example one wants to determine the lifetime of a thin epitaxial layer, it is possible to do that through a measurement dominated by scr generation, since the generation width in that case is the scr width [14]. If the measurement is dominated by qnr generation, then the appropriate width that is characterized is the minority carrier diffusion length L_n. But L_n is usually much longer than the epi layer thickness and diffusion length determination is poorly suited to characterize such layers. For generation rate measurements, it is reasonable to assume that room temperature characterization, in fact, determines τ_g. We see from Fig. 4, however, that conductance measurements are dominated by qnr generation even at room temperature and hence are characterized by τ_r or L_n, *not* by τ_g.

We will now present the effect of temperature, oxide thickness, doping density, and interface trapped charge density on C and G.

A. Effect of Temperature

The capacitance and conductance versus frequency as a function of temperature are shown in Fig. 5. The frequency increments between adjacent curves decrease with increasing temperature, due to qnr generation dominating at the higher temperatures. The upturn of the conductance at the higher frequencies is due to the frequency-dependent lifetime in our analysis.

To see the temperature dependence of the various frequencies, we have plotted ω_1, ω_2, and $\omega_{\rm mid}$ versus inverse temperature in Fig. 6. Just as in Fig. 4, here too, we see the scr generation component at temperatures below $T = 285$K, but at higher temperatures, qnr generation dominates. Extracting the activation energies E_A from Fig. 6 gives $E_A = 1.2$ eV for the high temperature and 0.6 eV for the low temperature regions. These values correspond to E_G and $E_G/2$ for Si. Recall that activation energies extracted from Arrhenius plots are energies for $T \rightarrow$ 0K. These various figures clearly show that measurements at room temperature or above *do not* characterize scr generation, i.e., the measurement depth is not that of the scr width, but rather is the minority carrier diffusion length.

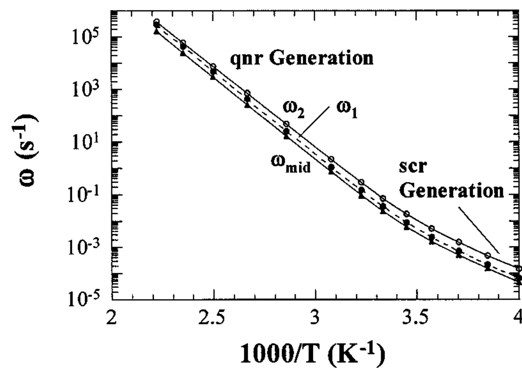

Fig. 6. Radian frequency versus inverse temperature showing the regions of scr and qnr generation domination. $\tau_{ro} = 20$ μs, $\tau_{go} = 1$ ms, $N_A = 10^{15}$ cm^{-3}, $t_{ox} = 100$ nm, $A = 1$ cm^2.

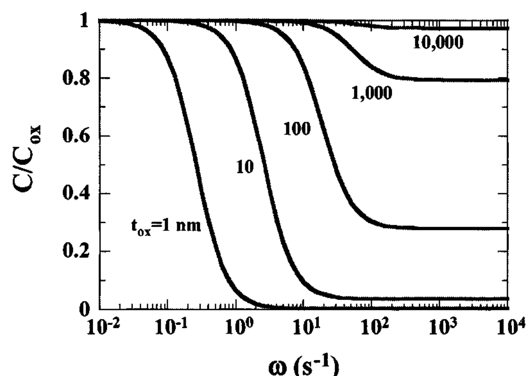

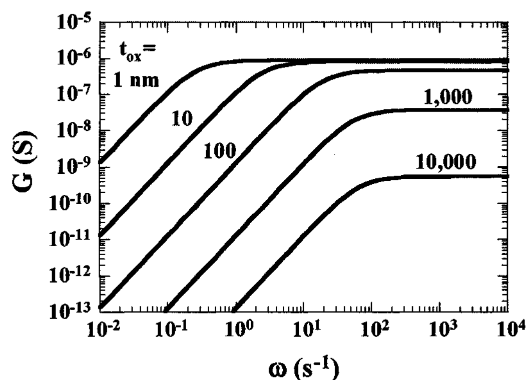

Fig. 7. Capacitance and conductance versus radian frequency as a function of oxide thickness. $\tau_{ro} = 20$ μs, $\tau_{go} = 1$ ms, $N_A = 10^{15}$ cm^{-3}, $T = 350$ K, $A = 1$ cm^2.

B. Effect of Oxide Thickness

What happens when the oxide thickness changes. For example, some measurements are made with Kelvin probes located several microns or even mm above the surface. Fig. 7 shows both C and G as a function of oxide thickness. Both figures show the mid frequency $\omega_{\rm mid}$ to approach ω_2, as predicted by $\omega_{\rm mid} = \omega_1\omega_2/(\omega_1 + \omega_2) = \omega_2/(1 + \omega_2/\omega_1) \approx \omega_2$ as $\omega_1 = G_N/C_{ox}$ becomes very high for thick oxides. The interpretation of the data becomes easier for thicker oxides, because ω_2 only depends on substrate parameters being independent of oxide parameters. The capacitance measurement becomes more difficult, however, because C/C_{ox} approaches unity as the oxide thickness increases and it is difficult to determine the mid frequency. Conductance measurements become more difficult, because the conductance decreases.

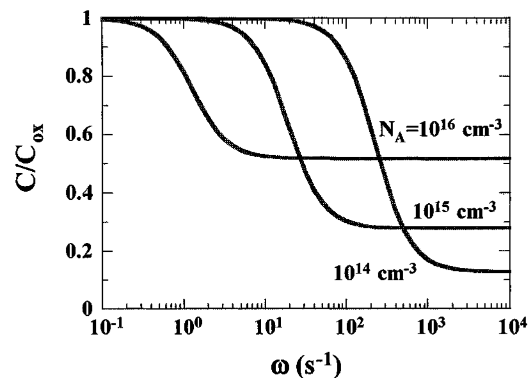

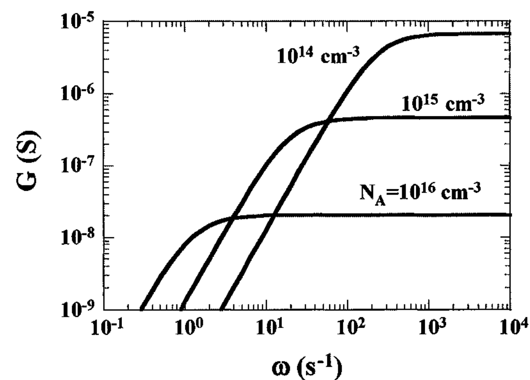

Fig. 8. Capacitance and conductance versus radian frequency as a function of doping density. $\tau_{ro} = 20$ μs, $\tau_{go} = 1$ ms, $t_{ox} = 100$ nm, $T = 350$ K, $A = 1$ cm^2.

C. Effect of Doping Density

With all break frequencies inversely proportional to the doping density, we find a strong dependence on N_A as illustrated in Fig. 8. This indicates that the doping density must be accurately known to extract the lifetime or diffusion length.

D. Effect of Lifetimes

As shown in Fig. 4, the device behavior is determined by qnr generation at room temperature and above. Hence, we would expect the recombination lifetime or diffusion length to have a major effect and the generation lifetime to have a minor effect. This is illustrated in Fig. 9. Varying τ_g from 10^{-5} to 10^{-3} s has little effect on these curves (not shown on the figures), as expected, since generation is dominated by qnr generation.

E. Effect of Interface Trap Density

Interface traps distort conventional MOS-C capacitance–voltage (C–V) curves, especially at low frequencies. Equations (2) and (3) include the effects of interface traps

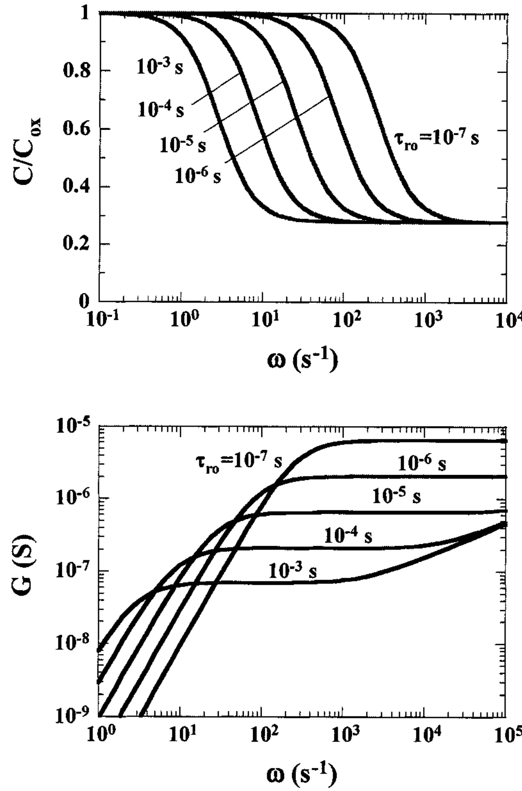

Fig. 9. Capacitance and conductance versus radian frequency as a function of lifetimes. $\tau_{go} = 1$ ms, $N_A = 10^{15}$ cm^{-3}, $t_{ox} = 100$ nm, $T = 350$ K, $A = 1$ cm^2.

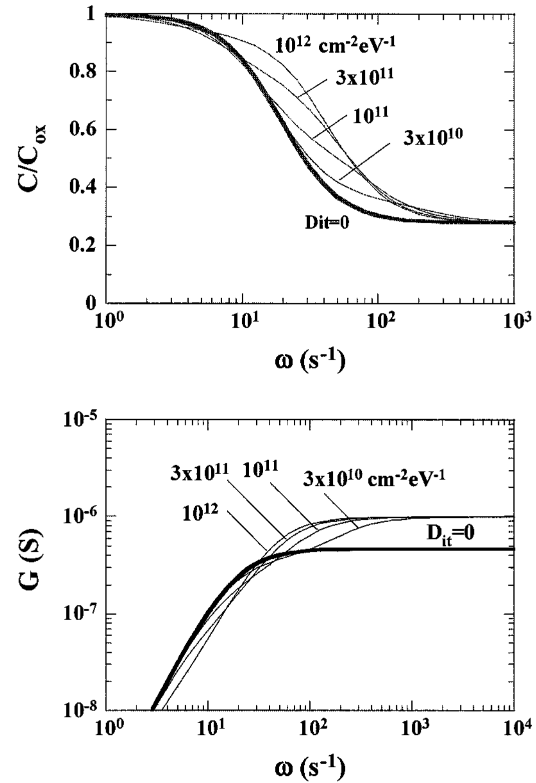

Fig. 10. Capacitance and conductance versus radian frequency as a function of interface trap density. $\tau_{ro} = 20\ \mu$s, $\tau_{go} = 1$ ms, $N_A = 10^{15}$ cm^{-3}, $t_{ox} = 100$ nm, $T = 350$ K, $R_{it} = 10^6\ \Omega$, $A = 1$ cm^2.

and we plot the theoretical results in Fig. 10. The higher the interface trap charge density, the more the curves distort.

F. Impedance Measurements

We have so far discussed capacitance and conductance, i.e., admittance, measurements. Sometimes, the voltage is measured, as for example, with a Kelvin probe. In that case, it is the voltage or impedance that is measured. The impedance of the circuit in Fig. 1 is given by

$$Z = R + jX \tag{16}$$

where R is the resistance and X the reactance. In terms of the conductance and the capacitance, the real and imaginary components of the impedance become

$$R = \frac{G}{G^2 + (\omega C)^2}; \qquad X = \frac{\omega C}{G^2 + (\omega C)^2}. \tag{17}$$

The resistance and reactance are plotted in Fig. 11. From the point of view of ease of determining a time constant, clearly the resistance is better. Its curve is well behaved with a well defined corner frequency ω_2 in contrast to the conductance corner frequency in Fig. 2 which gives ω_{mid}. The reactance X is more difficult to analyze, but one of the corner frequencies gives ω_{mid}.

The frequency behavior of R and X are shown in Fig. 12 as a function of temperature. Clearly the resistance data are more clearly defined than the reactance. The effects of oxide thickness, doping density, lifetime, and interface trap density are similar to those on conductance or capacitance.

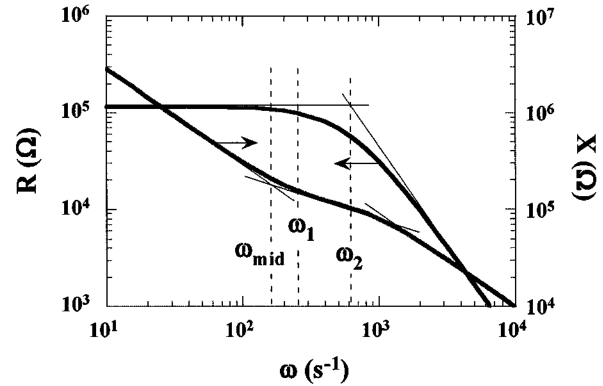

Fig. 11. Resistance and reactance as a function of radian frequency. $\tau_{ro} = 20\ \mu$s, $\tau_{go} = 1$ ms, $N_A = 10^{15}$ cm^{-3}, $t_{ox} = 100$ nm, $T = 370$ K, $A = 1$ cm^2.

During capacitance and conductance measurements, the low-level ac signal is usually provided by the measuring instrument. Resistance measurements are sometimes implemented with a Kelvin probe, where a modulated external light source provides the ac signal. Then it is important that optical carrier generation be sufficiently low not to provide carriers that add to the thermal generation rate. The thermal scr and optical generation rates are

$$G_{\mathrm{scr}} = \frac{qAn_iW}{\tau_g}; \qquad G_{opt} = qA\eta\Phi \tag{18}$$

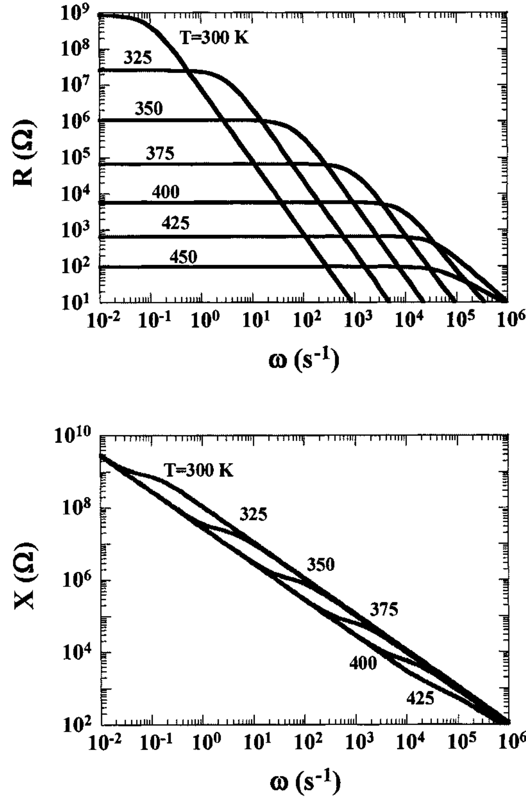

Fig. 12. Resistance and reactance versus radian frequency as a function of temperature. $\tau_{ro} = 20\ \mu$s, $\tau_{go} = 1$ ms, $N_A = 10^{15}$ cm^{-3}, $t_{ox} = 100$ nm, $A = 1$ cm^2.

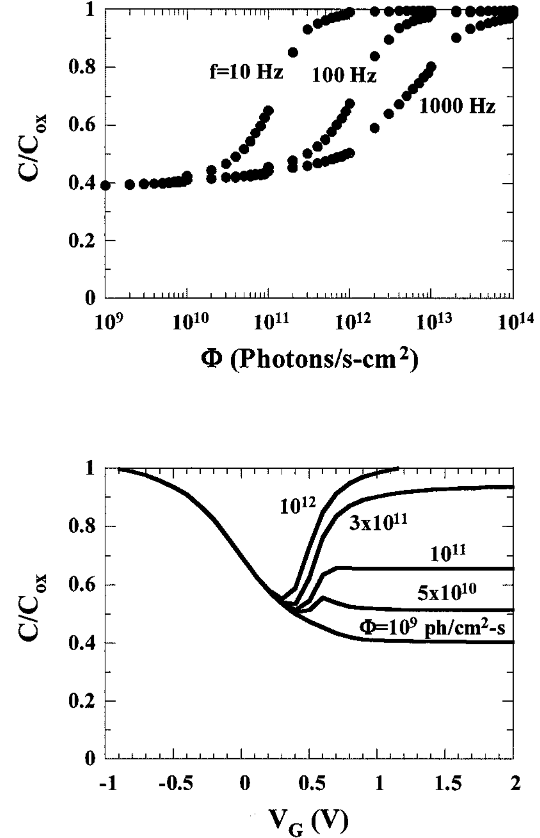

Fig. 13. C–V and C–Φ curves of an MOS capacitor. These curves were obtained from MEDICI modeling. Φ is the photon flux density. $\tau_{ro} = 1$ ms, $\tau_{go} = 1$ ms, $N_A = 10^{15}$ cm^{-3}, $t_{ox} = 100$ nm, $T = 300$ K.

where η is the quantum efficiency and Φ the photon flux density. For thermal generation to dominate, we require

$$\eta\Phi < \frac{n_i W}{\tau_g} \quad \text{or} \quad \Phi < \frac{n_i W}{\eta \tau_g}. \tag{19}$$

For Si at room temperature with $n_i = 10^{10}$ cm^{-3}, $W = 1\ \mu$m, $\tau_g = 1$ ms, and $\eta = 0.5$, we find $\Phi < 2 \times 10^9$ photons/s-cm^2.

To illustrate this effect, we show in Fig. 13 modeled $C/C_{ox} - V_G$ and $C/C_{ox} - \Phi$ curves of a MOS-C as a function of photon flux density. For low light levels, the expected high-frequency behavior is observed. As the light intensity is increased, we approach and finally reach the low-frequency curve. These figures show that the light level must indeed be very low in order for the light not to disturb the device operation. As predicted by (19), photon flux densities must be on the order of 10^9 photons/s-cm^2 or lower for this example.

IV. Theory—Modeling

In addition to the analytical theory discussed at length above, we have also carried out extensive modeling of the MOS capacitor, using the MEDICI model program. One set of C/C_{ox}–f and G–f curves determined from this model as well as from the analytical theory is shown in Fig. 14. We see good agreement of the curve shape, although there is some quantitative disagreement. It is not clear what causes this shift in the frequency in both sets of curves. It may be that MEDICI uses different parameters in the calculations. Furthermore, our analytical theory uses the depletion approximation in the space-charge region which is obviously a simplification. We also use $\phi_s = 2\phi_F$ as the inversion surface potential—another approximation. Nevertheless, we see the general agreement between our approximate analytical theory and detailed modeling.

V. Experimental Results

To test the theory proposed here, we have measured several MOS capacitors and compared the measured data to theory. Fig. 15 gives the data for an iron-doped and Fig. 16 for a gold-doped sample. Note the excellent agreement between theory and experiment for both the capacitance and the conductance data for both cases. We find the theoretical data to be independent of the generation lifetime for $\tau_g \geq 10^{-6}$ s, which is consistent with the earlier discussion, because both C and G are determined by qnr generation with scr generation playing a negligible role. This is not shown on the figures, but was determined during the simulations.

VI. Conclusions

We have developed a theory to interpret MOS capacitance and conductance data when measured versus frequency and have shown the C and G behavior as a function oxide thickness, doping density, recombination/generation lifetime, and interface trap density. One of the most important results of this work is that the frequency-dependent behavior at room temperature is governed by quasineutral region generation.

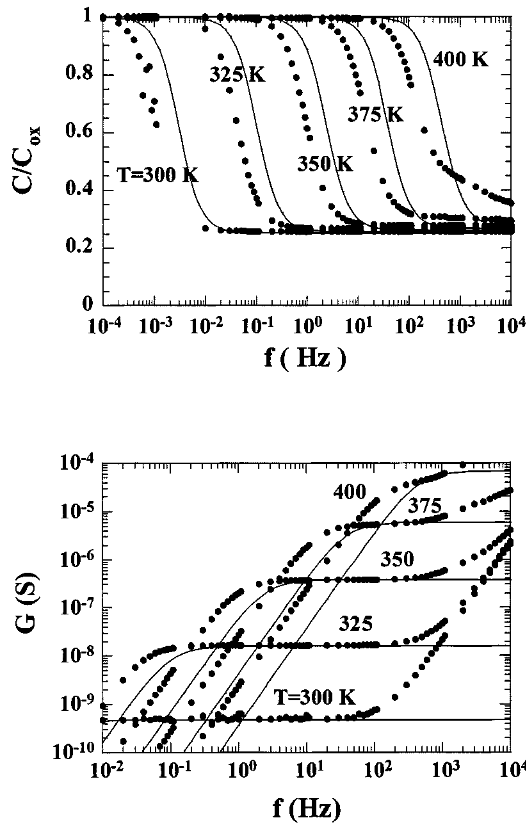

Fig. 14. MEDICI model (points) and analytical theory (lines) results. $\tau_{ro} = 20\ \mu$s, $\tau_{go} = 1$ ms, $N_A = 10^{15}$ cm^{-3}, $t_{ox} = 100$ nm, $A = 1$ cm^2.

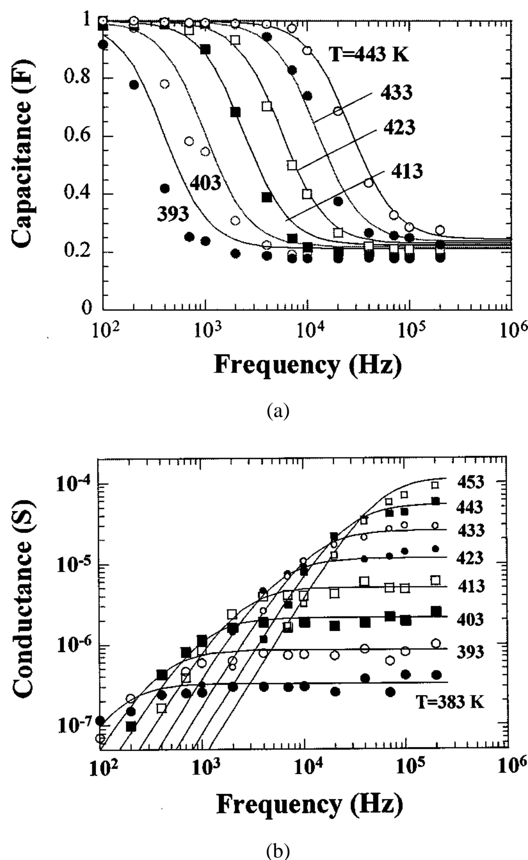

Fig. 15. Experimental (points) and calculated (lines) for Fe-doped Si. $\tau_{ro} = 1.3\ \mu$s, $\tau_{go} = 100\ \mu$s, $N_A = 1.25 \times 10^{15}$ cm^{-3}, $t_{ox} = 40$ nm.

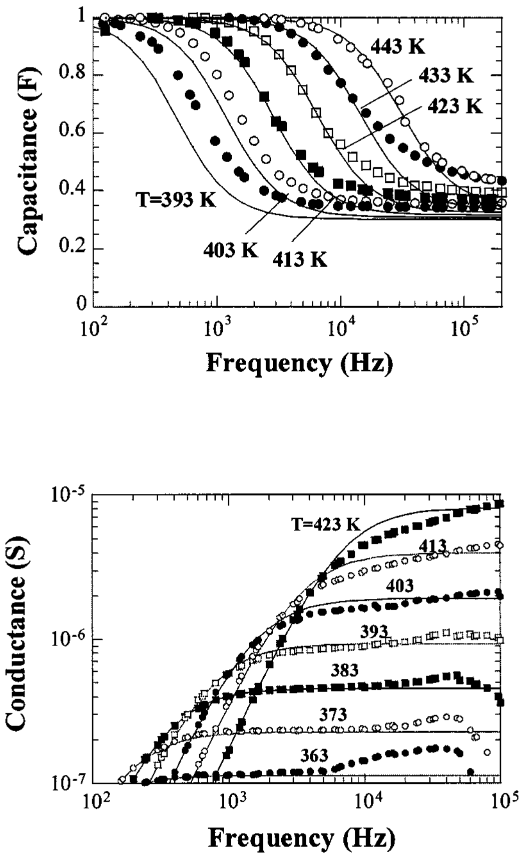

Fig. 16. Experimental (points) and calculated (lines) C–f for Au-doped Si. $\tau_{ro} = 3.5\ \mu$s, $\tau_{go} = 100\ \mu$s, $N_A = 1.5 \times 10^{15}$ cm^{-3}, $t_{ox} = 100$ nm.

This is surprising, because room-temperature pulsed MOS capacitor and diode leakage current measurements, frequently used for lifetime determination, are governed by space-charge region generation and generation lifetime and are localized to the width of the space-charge region. One application of these measurements is in the characterization of thin layers, e.g., epitaxial layers, denuded zones, or silicon-on-insulator. However, if quasineutral region generation dominates, then it is the minority carrier diffusion length that determines the characterization depth, not the space-charge region. But the diffusion length, being much longer than the widths of these layers, is a poor parameter to use in such cases.

REFERENCES

[1] D. K. Schroder, *Semiconductor Material and Device Characterization*. New York: Wiley, 1998.

[2] J. Lagowski, P. Edelman, M. Dexter, and W. Henley, "Non-contact mapping of heavy metal contamination for silicon IC fabrication," *Semicond. Sci. Technol.*, vol. 7, pp. A185–A192, 1992.

[3] C. Claeys, E. Simoen, A. Poyai, and A. Czerwinski, "Electrical quality assessment of epitaxial wafers based on p-n junction diagnostics," *J. Electrochem. Soc.*, vol. 146, pp. 3429–3434, Sept. 1999.

[4] D. K. Schroder, "Carrier lifetimes in silicon," *IEEE Trans. Electron Devices*, vol. 44, pp. 160–170, Jan. 1997.

[5] R. S. Nakhmanson, "Frequency dependence of the photo-EMF of strongly inverted Ge and Si MIS structures—I. Theory," *Solid-State Electron.*, vol. 18, pp. 617–626, July 1975.

[6] K. Lehovec and A. Slobodskoy, "Impedance of semiconductor-insulator-metal capacitors," *Solid-State Electron.*, vol. 7, pp. 59–79, Jan. 1964.

[7] S. R. Hofstein and G. Warfield, "Physical limitations on the frequency response of a semiconductor surface inversion layer," *Solid-State Electron.*, vol. 8, pp. 321–341, Mar. 1965.
[8] C. T. Sah, "The equivalent circuit model in solid-state electronics—III," *Solid-State Electron.*, vol. 13, pp. 1547–1575, Dec. 1970.
[9] E. H. Nicollian and J. R. Brews, *MOS Physics and Technology*. New York: Wiley, 1982.
[10] G. Baccarani, C. A. Baffoni, M. Rudan, and G. Spadini, "Majority- and minority-carrier lifetime in MOS structures," *Solid-State Electron.*, vol. 18, pp. 1115–1122, Dec. 1975.
[11] D. K. Schroder, J. D. Whitfield, and C. J. Varker, "Recombination lifetimes using the pulsed MOS capacitor," *IEEE Trans. Electron Devices*, vol. ED-31, pp. 462–467, Apr. 1984.
[12] J. P. McKelvey, *Solid-State and Semiconductor Physics*. New York: Harper & Row, 1966.
[13] D. K. Schroder, "The concept of generation and recombination lifetimes in semiconductors," *IEEE Trans. Electron Devices*, vol. ED-29, pp. 1336–1338, Aug. 1982.
[14] S. Y. Lee and D. K. Schroder, "Thin p/p^+ epitaxial layer characterization with the pulsed MOS capacitor," *Solid-State Electron.*, vol. 43, pp. 103–111, Jan. 1999.
[15] R. S. Nakhmanson, "Frequency dependence of the photo-EMF of strongly inverted Ge and Si MIS structures—II. Experiment," *Solid-State Electron.*, vol. 18, pp. 627–634, July/Aug. 1975.
[16] S. Y. Lee and D. K. Schroder, "Measurement time reduction for generation lifetimes," *IEEE Trans. Electron Devices*, vol. 46, pp. 1016–1021, May 1999.

Dieter K. Schroder (F'86) graduated from McGill University, Montreal, P.Q., Canada, and from the University of Illinois, Urbana.

He joined the Westinghouse Research Laboratories, Pittsburgh, PA, in 1968, where he was engaged in research on various aspects of semiconductor devices, including MOS devices, imaging arrays, power devices, and magnetostatic waves. He spent a year at the Institute of Applied Solid State Physics, Freiburg, Germany, in 1978. In 1981, he joined the Center for Solid State Electronics Research, Arizona State University, Tempe. His current interests are semiconductor materials and devices, characterization, low power electronics, and defects in semiconductors. He is the author of *Advanced MOS Devices* and *Semiconductor Material and Device Characterization* and has published over 120 papers.

Jae-Eun Park (M'96) received the B.S. degree from Kyung-pook National University, Tae-Gu, Korea and the M.S. degree from Arizona State University, Tempe, in 1988. He is currently pursuing the Ph. D. degree.

He was engaged in research on SiGeC HBT's, field emission device and carrier lifetime characterization in Si. His current interests include hot carriers, carrier lifetime characterization and reliability of nonvolatile memory devices.

Mr. Park is a member of Phi Kappa Phi.

Suat-Eng Tan was born in Johor, Malaysia. She received the B.S. degree from National Taiwan University, Taiwan, and the Ph.D. degree from National University of Singapore, Singapore, both in electrical engineering, in 1993 and 1997, respectively. Her Ph.D. research focused on hot-carrier effects in submicron MOS devices.

She joined the Department of Electrical Engineering, Arizona State University, Tempe, as a Post-Doctoral Researcher. During the summer of 1999, she was a Visiting Researcher at Mitsubishi Silicon America, Salem, OR. She is now a Senior Process Integration Engineer at WaferTech, Portland, OR. Her current research interests include ULSI/VLSI device fabrication, defect studies, characterization and simulation of hot-carrier effects, and carrier lifetimes in semiconductor. She has published more than 10 journal and conference papers in these fields.

Byoung D. Choi received the B.S. and M.S. degrees in physics from Kyung Hee University, Seoul, Korea, in 1988 and 1990, respectively, and the M.S. degree in electrical engineering from Arizona State University (ASU), Tempe, in 1998. Currently, he is pursuing the Ph.D. degree in electrical engineering at ASU.

He has been a Graduate Research Associate under Dr. D. K. Schroder in electrical engineering at ASU since June 1998. His research involves MOS devices, defects in semiconductor, carrier lifetime measurement, and gate oxide integrity.

Seigo Kishino was born in Okayama, Japan, on November 1, 1938. He received the B.S. degree from Osaka University, Japan, in 1962, and the Ph.D. degree from the University of Tokyo, Japan, in 1972.

In 1962, he joined the Central Research Laboratories, Hitachi, Ltd., Tokyo, where his experience included the study of X-ray diffraction and material characterization of semiconductors. Between 1977 and 1980, he was a member of the Cooperative Laboratories of the VLSI Technology Research Association, Kawasaki, Japan, where he worked on microdefects in silicon crystals and their application to gettering techniques. Since 1987, he has been Professor in the Department of Electronics, Faculty of Engineering,Himeji Institute of Technology, Himeji, Japan. He is currently working on the contactless electrical characterization of localized states in semiconductors, especially in SOI materials.

Dr. Kishino is a member of the Japan Society of Applied Physics and the Institute of Electrical Engineering of Japan.

Haruhiko Yoshida was born in Hyogo, Japan, on May 5, 1966. He received the B.S., M.S., and Ph.D. degrees in electronics from Himeji Institute of Technology, Himeji, Japan, in 1989, 1991, and 1994, respectively.

In 1994, he joined the Department of Electronics, Faculty of Engineering, Himeji Institute of Technology, where he is currently a Lecturer. His work includes deep level characterization of MOS devices using isothermal capacitance transient spectroscopy and the development of contactless transient spectroscopy. He is currently working on the contactless characterization of localized states in SOI material.

Dr. Yoshida is a member of the Japan Society of Applied Physics.